Hindawi Publishing Corporation
Journal of Nanomaterials
Volume 2014, Article ID 468271, 11 pages
http://dx.doi.org/10.1155/2014/468271

Research Article

Improvement of Orange II Photobleaching by Moderate Ga^{3+} Doping of Titania and Detrimental Effect of Structural Disorder on Ga Overloading

Václav Štengl,[1] Jiří Henych,[1] Michaela Slušná,[1] Tomáš Matys Grygar,[1] Jana Velická,[1] and Martin Kormunda[2]

[1] *Material Chemistry Department, Institute of Inorganic Chemistry AS CR v.v.i., 25068 Řež, Czech Republic*
[2] *Department of Physics, Faculty of Science, J.E.Purkyně University in Ústí nad Labem, 400 96 Ústí nad Labem, Czech Republic*

Correspondence should be addressed to Václav Štengl; stengl@iic.cas.cz

Received 7 August 2013; Revised 5 January 2014; Accepted 5 January 2014; Published 26 February 2014

Academic Editor: Do K. Kim

Highly photoactive Ga^{3+}-doped anatase modification of titania was prepared by homogeneous hydrolysis of aqueous solutions mixture of titanium oxo-sulphate $TiOSO_4$ and gallium(III) nitrate with urea. Incorporation of Ga^{3+} into the anatase lattice has a clear positive effect on the photocatalytic activity under UV and Vis light irradiation up to a certain extent of Ga. Ga^{3+} doping decreased the size of the crystallites, increased surface area, and affected texture of the samples. Higher amount of gallium leads to the formation of a nondiffractive phase, probably photocatalytically inactive. The titania sample with 2.18 wt.% Ge^{3+} had the highest activity during the photocatalysed degradation in the UV and visible light regions; the total bleaching of dye Orange II was achieved within 29 minutes. Ga concentration larger than 5% (up to 15%) significantly inhibited the growth of the anatase crystal domains which formed the nondiffractive phase content and led to remarkable worsening of the photobleaching efficiency.

1. Introduction

Nowadays, attempts by numerous synthesis chemists are focused on the increase of the photocatalytic activity of titanium dioxide so it can be commercially used for various applications, such as self-cleaning coating and air and water purifiers. An important factor for the commercial use of TiO_2 as photocatalyst is its low cost. The photocatalysts performance can be improved basically in two ways. Firstly by ion doping to change the electronic structure or by finding a suitable compromise between morphology, structural parameters, and texture of photocatalyst because, for instance, shape of particles and their size fundamentally affect photocatalytic properties. Optimal particle size for photocatalytic applications lies somewhere around 40–80 nm. Too small particles (below 20 nm) [1] or vice versa too large particles (>100 nm) [2] have lower activity. Last but not least the crystallinity of particles plays an important role, because the high content of the amorphous domains has detrimental effect on the performance.

The textural parameters, that is, a porosity of the sample, influence photocatalytic activity much more than its surface area, as could be implicated for instance from mesoporous TiO_2 samples prepared by homogeneous hydrolysis of titanyl sulphate $TiOSO_4$ with urea in the presence of anionic and cationic surfactants hexadecyltrimethylammonium bromide $C_{16}H_{33}N(CH_3)_3Br$ (CTAB) and sodium dodecylbenzene sulphonate $C_{18}H_{29}NaSO_3$ (SDBS) [3]. The surfactants changes morphology and texture of titania: the original spherical agglomerates are disintegrated and open structures resembling clusters of corals are formed instead. Their maximum pore size is up to 10 nm depending on the surfactant concentration. The other way to increase the efficiency of photocatalysis is an extension of photocatalyst light absorption to the visible range, that is, $\lambda > 400$ nm. Highly desirable is substitution into the crystal lattice of TiO_2.

Depending on the nature of the element two major types of dopants, P-type and N-type, can be discerned. A P-type doping is achieved by incorporating the cation of valency lower than Ti^{4+}; these include In^{3+} [4], Al^{3+}, Cr^{3+}, Ga^{3+}, La^{3+}, and Y^{3+} [5], whilst dopants of N-type are cations of a valency higher than 4, for example, Nb^{5+}, Ta^{5+} [6], Sb^{5+}, W^{5+} [7], and Mo^{6+} [8]. The main goal of doping is a bathochromic shift, moving an absorption edge from the UV to the visible light area, thus reducing the band gap. Besides the band gap narrowing, further inner layers in a restricted zone can be incorporated, also allowing the absorption of visible light.

Banerjee et al. [9] reported on the oxidation of organic dye (Rhodamine B) into nontoxic inorganic products under UV irradiation using a Ga-doped TiO_2 synthesised by sol-gel technique. Pure TiO_2, single-doped, and Ga+N codoped titania nanoparticles were successfully prepared by sol-gel method. Detailed analysis showed that the resulting TiO_2 has the anatase structure. Nitrogen and gallium atoms were incorporated into the titanium dioxide lattice and the Ga+N codoped TiO_2 exhibited the highest absorption of visible light [10]. Anatase-type titania nanoparticles codoped with niobium and gallium ($Ga_XTi_{1-2X}Nb_XO_2$ solid solutions in the range of $X = 0$–0.20) were formed from precursor solutions of $TiOSO_4$, $NbCl_5$, and $Ga(NO_3)_3$ under hydrothermal conditions at 180°C for 5 h using the hydrolysis of urea. The effect of dopant materials on the structure, crystallite growth, photocatalytic activity, and phase stability of anatase-type TiO_2 was investigated. The lattice parameters a_0 and c_0 of anatase slightly and gradually increased with increase in niobium and gallium content doped into TiO_2 [11]. Iodine-doped titania photocatalysts were improved by doping with gallium and the resulting physicochemical properties and photocatalytic activity were investigated. Gallium ions played a decisive role in retarding the anatase-rutile phase transformation, extending the absorption spectrum and creating oxygen vacancies for photoelectron trapping to prevent the $e^- - h^+$ recombination process [12]. Copper- and gallium-doped titania photocatalysts prepared by means of sol-gel technique and analysed by XRD were found to contain specific crystalline phases of anatase, β-Ga_2O_3, and Cu_2O, which allowed inferring on the doping phenomena of both transition and posttransition metals [13].

In this work, we present preparation of Ga^{3+} substitutionally doped titania, nanostructured materials with high photocatalytic activity, obtained by homogeneous hydrolysis of $TiOSO_4$ and $Ga(NO_3)_3$ with urea. The samples were tested successfully for photocatalytic degradation of Orange II dye in an aqueous slurry under irradiation at wavelengths of 365 nm and >400 nm.

2. Experimental Section

2.1. Preparation of Samples. All chemical reagents used in the present experiments were obtained from commercial sources and were used without further purification. Titanium oxo-sulphate $TiOSO_4$, urea $CO(NH_2)_2$, and metal Ga were supplied by Sigma-Aldrich, Czech Republic. The gallium(III) nitrate $Ga(NO_3)_3$ was prepared by a stoichiometric reaction of metal Ga and nitric acid HNO_3. Homogeneous hydrolysis of $TiOSO_4$ and $Ga(NO_3)_3$ in aqueous solutions with urea as a precipitation agent was used for doped titania preparation. In a typical process, a predefined amount of $TiOSO_4$ (see Table 1) was dissolved in 100 mL of hot distilled water acidified with 98% H_2SO_4. The pellucid liquid was diluted into 4 L of distilled water, added defined amount of $Ga(NO_3)_3$ and 300 g of urea. The mixture was heated at 98°C under stirring for 6 h until pH reached 7.2. The formed precipitate was washed using decantation until conductivity of 10 μS was reached, filtered off, and dried at 105°C. Eight Ga^{3+} doped titania samples denoted as TiGa001, TiGa005, TiGa010, TiGa020, TiGa050, TiGa080, TiGa100, and TiGa120 were prepared.

2.2. Characterisation Methods. Diffraction patterns were collected with a diffractometer PANalytical X'Pert PRO equipped with a conventional X-ray tube (Cu Kα radiation, 40 kV, 30 mA) and a linear position sensitive detector PIXcel with an antiscatter shield. A programmable divergence slit set to a fixed value of 0.5 deg, Soller slits of 0.02 rad, and mask of 15 mm were used in the primary beam. A programmable antiscatter slit set to fixed value of 0.5 deg, Soller slit of 0.02 rad, and Ni beta-filter were used in the diffracted beam. Qualitative analysis was performed with the DiffracPlus Eva software package (Bruker AXS, Germany) using the JCPDS PDF-2 database [14]. For quantitative analysis of XRD patterns Diffrac-Plus Topas (Bruker AXS, Germany, version 4.1) with structural models based on ICSD database [15] was used for Rietveld refinement. This program permits to estimate the weight fractions of crystalline phases and mean coherence length by means of Rietveld refinement procedure. The internal standard addition method with rutile (10 wt.%) was used for nondiffractive phase determination [16].

Rietveld refinement is based on a full-profile fitting of XRD pattern to calculated diffraction patterns of individual mineral phases. The presence of "amorphous" (=non-diffracting) components is determined from the misfit of the percentage of the internal standard retrieved by the refinement and the real percentage in the mixture (the larger the content of nondiffracting components, the more the calculated internal standard percentage exceeds the real percentage in the analysed mixture).

The surface areas of samples were determined from nitrogen adsorption-desorption isotherms at liquid nitrogen temperature using a Coulter SA3100 instrument with 15 min outgas at 150°C. The Brunauer-Emmett-Teller (BET) method was used for surface area calculation [17]; the pore size distribution (pore diameter, pore volume, and micropore surface area of the samples) was determined by the Barrett-Joyner-Halenda (BJH) method [18].

Scanning electron microscopy was performed with JEOL JSM-6510 equipped with an energy dispersive X-ray spectrometer (EDS). Specimens for morphological investigations were prepared by droplet evaporation of samples dispersion on a carbon-supported SEM target. The specimens have been imaged in the low-vacuum mode using accelerating voltage of 30 kV.

Table 1: Experimental conditions, parameters from Rietveld refinement, surface area, and porosity.

Sample	$Ga(NO_3)_3$ (g)	XRF Ga^{3+} (wt.%)	Anatase phase (wt.%)	Non-diffractivephase (wt.%)	Cell param. a (Å)	Cell param. c (Å)	Cell vol. change $\Delta V/V_0$ (%)	Cryst. size (nm)	Surface area (m^2g^{-1})	Total pore volume (cm^3g^{-1})	Average pore size (nm)
TiGa001	0.128	0.51	93.43	6.57	3.7964	9.5059	0.03	7.2	266.8	0.2349	9.6
TiGa005	0.64	0.98	92.68	7.32	3.7965	9.5046	0.02	6.9	258.7	0.2239	7.6
TiGa010	1.28	2.18	92.95	7.05	3.7989	9.5037	0.08	6.6	242.9	0.2888	25.9
TiGa020	2.56	4.28	93.01	6.99	3.7999	9.5059	0.13	5.2	260.6	0.2734	25.3
TiGa050	6.4	5.66	86.53	13.47	3.8030	9.5217	0.37	5.2	279.2	0.2481	7.8
TiGa080	10.24	13.60	79.52	20.48	3.8104	9.494	0.28	5.1	279.3	0.2426	10.9
TiGa100	12.8	12.50	74.75	25.25	3.8143	9.4982	0.42	4.3	306.0	0.2727	8.2
TiGa120	15.36	18.69	63.35	36.65	3.8156	9.4888	0.36	4.4	300.0	0.2527	10.1

The Raman spectra were acquired with DXR Raman microscope (Thermo Scientific) with 532 nm (6 mW) laser; 32 two-second scans were accumulated with laser 532 nm (6 mW) under 10x objective of Olympus microscope.

Infrared spectra were recorded using a Nicolet Impact 400D spectrometer over the range of approximately 4000–500 cm^{-1} equipped with a DRIFT cell (500 scans, resolution 4 cm^{-1}).

A Perkin Elmer Lambda 35 spectrometer equipped with a Labsphere RSAPE-20 integration sphere with $BaSO_4$ as a standard was used for the diffuse reflectance UV/Vis spectra. The spectra were recorded in the diffuse reflectance mode and transformed to absorption spectra through the Kubelka-Munk function [19, 20]:

$$f(R) = \frac{(1-R)^2}{2R}, \quad (1)$$

where $f(R)$ is absorbance and R is the reflectance of an "infinitely thick" layer of the solid.

The XPS apparatus was equipped with a SPECS X-Ray XR50 (Al cathode 1486.6 eV) and SPECS PHOIBOS 100 Hemispheric Analyzer with a 5-channel detector. A background pressure in XPS during the measurements was under 2×10^{-8} mbar. XPS survey-scan spectra were made at 40 eV pass energy; the energy resolution was set to 0.5 eV. While individual high-resolution spectra were taken at 10 eV pass energy with 0.05 eV energy steps. A software tool CasaXPS was used to fit the high-resolution multicomponent peaks. The proper surface charge compensation was done by fitting C–C, C–H component of C 1s peak to reference binding energy 284.5 eV. The atomic concentration of compounds was evaluated with relative sensitivity factors (RSF) defined in the standard table of the CasaXPS software.

2.3. Photocatalytic Activity Tests. Photocatalytic activity of samples was assessed from the photobleaching kinetics of Orange II dye (sodium salt of 4-[(2-hydroxy-1-naphthenyl)azo]-benzene sulphonic acid) in 1000 mL of aqueous slurries using a self-constructed photoreactor [21]. It consists of a stainless steel cover and an inner quartz tube with a fluorescent lamp (Narva) with power of 13 W producing a light intensity of ~3.5 mW/cm^2. We used either a lamp with a commercial name "Black Light" (365 nm) or "Warm White" (emission spectrum > 400 nm). The emission spectra of both sources were shown in [22]. A portion of 0.5 g photocatalyst was dispersed in an ultrasonic bath (300 W, 35 kHz) for 10 min before kinetic tests; the actual way of dispersing the oxide plays a crucial role in obtaining reproducible results of the kinetic tests. The pH was kept at a value of 7.0. Orange II dye solution was circulated by means of a membrane pump through a flow cell. The concentration of Orange II in the suspension was determined by measuring absorbance at 480 nm with Vis spectrophotometer ColorQuestXE. The suspension contained 5 mmol of the dye at the beginning of the kinetic test, which is a substantial excess over what can be adsorbed by the catalyst. Maximal adsorption of structurally similar azo dyes Orange G and Methyl Orange is <10 μmol per gram of P25 titania [23]; hence, in our experimental setup the azo dye amount exceeds the titania adsorption capacity by about two orders of magnitude. None of the two used light sources can photobleach Orange II without a photocatalyst. The kinetic experiment started by switching on the light source after the spectral signal of the Orange II in the suspension reached a steady state; this actual initial signal was taken as a measure of the initial concentration of the dye. The sorption of the dye on the catalysts is hence irrelevant for the evaluation of the kinetic experiments.

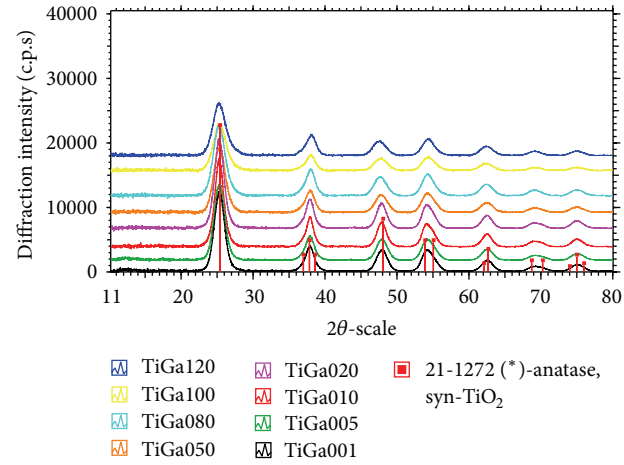

FIGURE 1: XRD pattern of prepared Ga^{3+}-doped titania samples.

3. Results and Discussions

3.1. Structural Analysis. The XRD patterns of the Ga^{3+}-doped titania samples are shown in Figure 1. Only the diffraction lines of anatase (ICDD PDF 21-1272) can be seen. The crystallite size, anatase and nondiffractive phase contents, and cell parameters a and c of anatase (calculated by Rietveld refinement) are presented in Table 1. The crystallite size of anatase decreases from 7.2 nm to 4.4 with growing gallium content, which is also related to an increase of the nondiffractive phase. This phenomenon can influence the photocatalytic activity of as-prepared samples. The ionic radius of Ga^{3+} (0.062 nm) [24] is only slightly larger than ionic radius of Ti^{4+} (0.0605 nm) [25] and gallium could hence substitute Ti^{4+} in the crystal lattice. At least partial incorporation of Ga^{3+} into the anatase lattice was suggested from the relative change of the cell volume (ΔV) compared to undoped TiO_2 (V_0) prepared by the same synthesis method [26]. The volume grew with increasing dopant concentration (see Table 1).

The nondiffractive fraction of the doped titania increased linearly with growing Ga content (see Table 1): linear regression of the percentage of nondiffractive portion of the samples versus Ga content formally expressed as Ga_2O_3 with a slope close to 1 (1.2-1.3 depending on the Ga concentration range) suggests that Ga addition promotes the growth of the nondiffractive portion of the samples. It is probable that the nondiffractive portion of the specimens is Ga-rich, but it must also contain some Ti (the slope of nondiffractive content versus formal Ga_2O_3 percentage is >1).

Because the percentage of the nondiffractive content was estimated by Rietveld analysis, that is, from decrease of the diffraction intensity of the target anatase with respect to internal standard, it may alternatively reflect also decrease of the structural order of the doped titania; high concentration of defects stochastically disordering atomic positions would also decrease the diffracted intensity.

Characterization of nanosized materials by classic material characterization methods has serious pitfalls. The integral intensities of diffraction lines become lower when crystallite size decreases to a few nanometres or less. Very small crystallites (size of very few nanometers) could be almost nondiffractive and could then be considered as "amorphous phase" in sense of X-ray diffraction. X-ray diffraction could therefore provide misleading results. This was recently noted and elaborated by Weidenthaler [27] Ga addition truly hindered particle growth and led to very small particles, of which the smallest are nondiffractive.

The addition of gallium to anatase slightly increased the surface area, which is connected to lowering the crystallite sizes shown in Table 1. The Barrett-Joyner-Halenda (BJH) pore-size distribution plot and nitrogen adsorption/desorption isotherms of the as-prepared Ga-doped TiO_2 are shown in Supplementary Figures S1 (see Supplementary Material available online at http://dx.doi.org/10.1155/2014/468271). According to IUPAC notation [28], microporous and macroporous materials have pore diameters of less than 2 nm and greater than 50 nm, respectively; the mesoporous category thus lies in the middle. All the prepared samples have a type IV isotherm, which is mainly characteristic for mesoporous materials [29]. The maximum of pore size (~3 nm) for all prepared samples is in-between mesoporous and microporous solids. However, samples TiGa001, TiGa005, TiGa050, TiGa080, and TiGa100 have significantly narrower pore size distribution with higher amount of smaller pores. The content of very small pores decreases photocatalytic activity. The samples TiGa010, TiGa020, and TiGa120 have a maximum of pores size at 5 and 60 nm, respectively; the mesoporosity enhanced photocatalytic activity. It is commonly accepted that mesoporous TiO_2 with a large surface area is the best photocatalyst, since a larger surface area offers more active adsorption sites. However, it is difficult to explain the high activity of mesoporous TiO_2 based solely on its surface area [30].

3.2. Other Analyses. Supplementary Figure S2 shows the IR spectrum of the Ga-doped TiO_2. The broad absorption band at ~3400 cm^{-1} and the band at 1641 cm^{-1} correspond to the surface-adsorbed water and the hydroxyl groups [31]. The band at 1445 cm^{-1} can be assigned to the asymmetric stretching mode of C–O bond of adsorbed carbonate ions on the TiO_2 surfaces, formed probably by the adsorption of CO_2 from air [32] or remnants from the synthesis (CO_2 is the main decomposition product of urea). Surface-adsorbed sulphate ions are probably $TiOSO_4$ residue responsible for a small band at 1100 cm^{-1} [33]. The peak located at ~468 cm^{-1} in the FT-IR spectrum is likely due to the vibration of the Ti–O bond [34]. The band at 905 cm^{-1} can be assigned analogously to the stretching vibration of Ti–O–Ga [35].

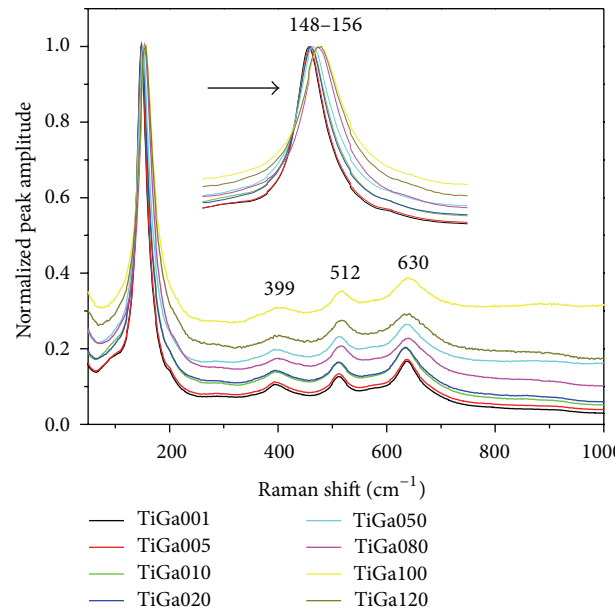

FIGURE 2: The Raman spectra of prepared Ga^{3+}-doped titania.

The Raman spectra of the Ga-titania series are presented in Figure 2. The specific vibration modes are located at 148 cm^{-1} (Eg), 399 cm^{-1} (B1 g), 512 cm^{-1} (B1g + A1g), and 630 cm^{-1} (Eg), indicating the presence of the anatase phase in all of these samples. The absence of Raman active band around 318 cm^{-1}, which would be characteristic for Ga_2O_3 [9], shows the absence of crystalline gallium oxide. Unfortunately, neither Raman spectroscopy is sufficiently sensitive to amorphous (or highly defective) phases. The red shift of specific vibration Eg of the anatase structure from 148 cm^{-1} to 156 cm^{-1} (the inset in Figure 2) with the increasing gallium content confirms, however, at least partial incorporation of Ga^{3+} in the anatase lattice [36].

The XPS survey spectrum of samples TiGa001 and TiGa010 and the high resolution XPS spectra of Ti 2p, O1s, and Ga2p are shown in Supplementary Figure S3. In the Ti 2p spectrum the Ti 2p3/2 and Ti 2p1/2 were identified at binding energies 458.7 eV and 464.4 eV; these arise from the presence of Ti^{4+} in pure anatase [37]. The O1s peak can be deconvoluted into Ti^{4+}–O bond at 530.0 eV and Ti–OH bond at 531.6 eV. The presence of Ti–OH bond is important for photocatalytic activity due to the production of large amounts of OH• radicals [38] and due to modified surface hydrophilicity of titania. The Ga2p 3/2 orbital for sample TiGa010 was located at binding energy of 1118 eV [39]. In TiGa001 sample the Ga concentration is below the XPS detection limit; that is, Ga was incorporated in the structure (it was not enriched on the titania surface). The traces of metallic indium were detected in survey spectrum; the source was probably in metal Ga, used in the $Ga(NO_3)_3$ preparation.

HRTEM images of gallium-doped titania nanocrystals incorporated into anatase particles are shown in Figure 3.

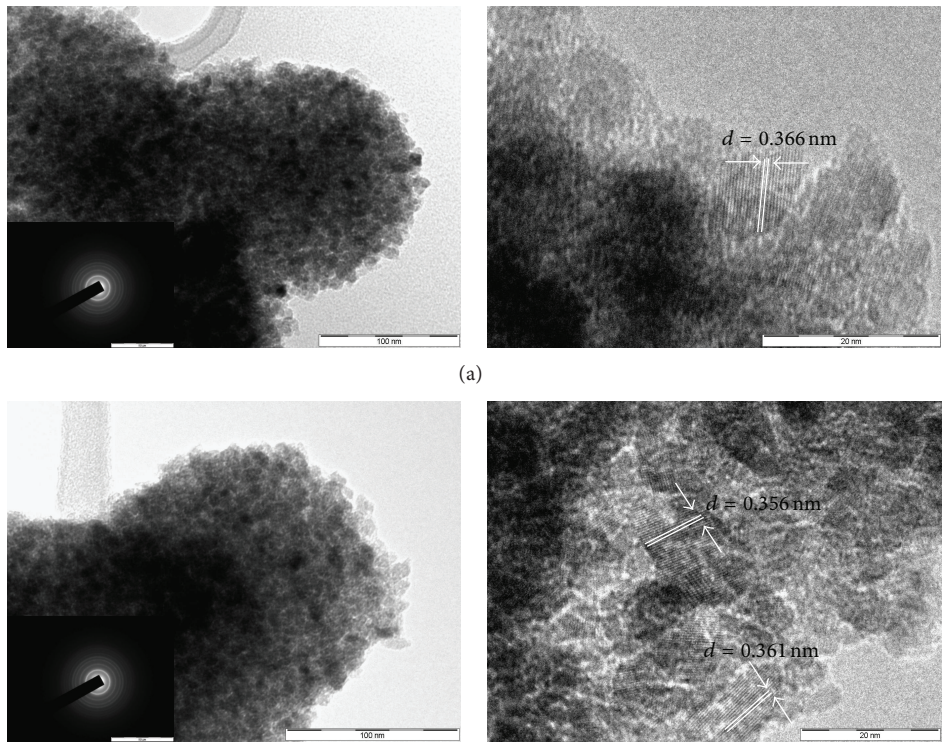

Figure 3: HRTEM of samples (a) TiGa001 and (b) TiGa020.

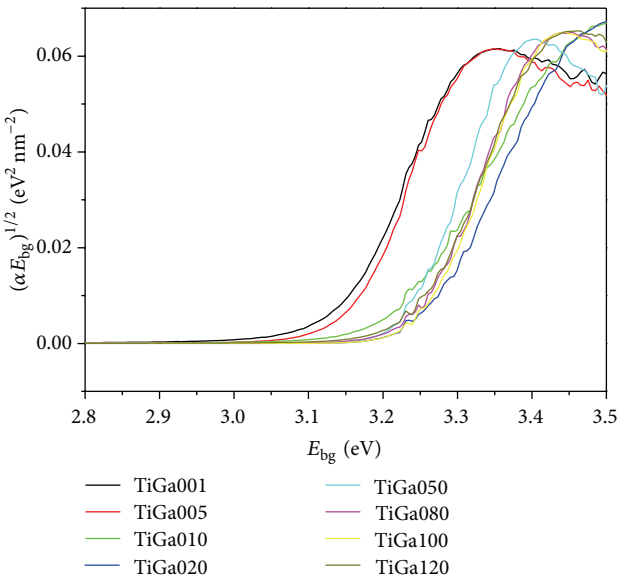

Figure 4: Band-gap energy of Ga^{3+}-doped TiO_2.

The interlayer spacing along the [101] direction of the anatase is increased from $d = 0.356$ nm in TiGa001 to $d = 0.366$ nm in TiGa020 due to incorporation of Ga^{3+} in to anatase crystal lattice. The HRTEM images clearly show very well crystalline materials, which contain no amorphous domains. The selected area electron diffraction patterns (SAED), presented in Supplementary Figures 4 and 5, obtained by the Process Diffraction program, showed that the structure of all samples is anatase (ICDD PDF 21-1272).

The electronic bands of annealed titania samples were studied using UV-Vis diffuse reflectance spectroscopy. Supplementary Figure S6 presents absorption spectra of the as-prepared titania samples. The reflectance data obtained were a percentage reflectance relative to a nonabsorbing material ($BaSO_4$). The Kubelka-Munk theory is generally used for the analysis of diffuse reflectance spectra of weakly absorbing samples [19]. Compared with the pure titania sample (sample notation TiP), weak absorption edge red shift (bathochromic shift) is observed with samples denoted as TiGa001 and TiGa005 other samples, by contrast, have a weak blue shift. The method of UV-Vis diffuse reflectance spectroscopy was employed to estimate the band-gap energies of the heated titania samples. Firstly, to establish the type of band-to-band transition in these synthesised samples, the absorption data were fitted to equations for indirect band-gap transitions. The minimum wavelength required to excite an electron depends on the band-gap energy E_{bg} which is commonly estimated from UV-Vis absorption spectra by the linear extrapolation of the absorption coefficient to zero using the following equation:

$$\alpha(h\nu) = R\left(h\nu - E_{bg}\right)n, \tag{2}$$

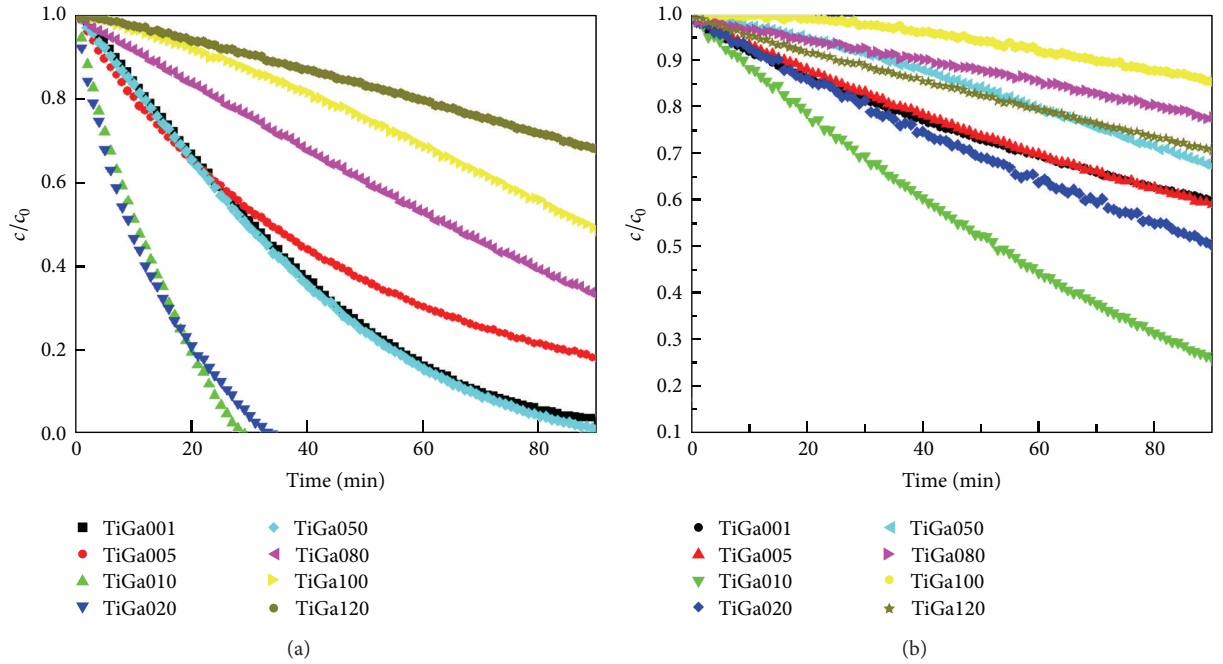

Figure 5: Kinetics of photodegradation of Orange II dye under (a) 365 nm and (b) over 400 nm.

where A is the absorption according to (1), $h\nu$ is the photon energy in eV calculated from the wavelength λ in nm [40, 41]

$$h\nu = \frac{1239}{\lambda}, \tag{3}$$

and the exponent n in (2) describes the type of the electronic transition in bulk semiconductors: $n = 2$, 1/2, 3, and 3/2 for indirect allowed, direct allowed, indirect forbidden, and direct forbidden transitions, respectively [42].

The energy of the band gap was calculated by extrapolating a straight line (a regression line according to linearised form of (2)) to the x axis ($\alpha = 0$); then $E_{bg} = h\nu$ [43]. Figure 4 shows the $(Ah\nu)^{1/2}$ versus photon energy for an indirect band-gap transition. The resulting extrapolated values of E_{bg} for the indirect transitions are listed in Table 1. The value of ~3.10 eV for nondoped titania is reported in the literature for pure anatase nanoparticles [44, 45]. The value of band-gap energy varies in range ~3.1–3.25 eV. Light absorption is highly different by changing content of Ga^{3+} in the samples. The samples with moderate Ga^{3+} content (TiGa001 and TiGa005) exhibited a red shift of absorption edge up to 400 nm, which corresponds to the value of band-gap energy ~3.1 eV. This shift may be due to incorporation of Ga^{3+} into the structure of TiO_2. With increasing gallium content, however, the opposite trend, a blue shift of the absorption edge was observed. It may be relevant that nascent Ga_2O_3 has a band-gap energy 4.8 eV [46], and hence the hypothetic Ga-rich nondiffractive component could also have broader bandgap than anatase. A similar blue shift due to formation of a nondiffractive phase has already been observed in Ge^{4+}-doped TiO_2 [47].

3.3. Kinetic Tests. For the formal kinetic description of the Orange II photobleaching on the Ga^{3+}-doped titania the Langmiur-Hinshelwood equation can be used [47, 48]. The results are shown in Figure 5 and Table 2. Doping by Ga^{3+} increases the photocatalytic activity in both the UV and visible regions in comparison to undoped sample (with apparent rate constants $k = 0.0073$ and $k = 0.0020\,\text{min}^{-1}$ under UV and visible light irradiation, resp.) [7]. The low activity of the lower-doped sample is due to a low crystallinity and varied structural defects conventionally assumed to act as recombination centres resulting in an insufficient separation of hole-electron couples [49]. The lower photocatalytic activity of the samples TiGa001, TiGa005, TiGa050, TiGa080, and TiGa100 is probably caused by their microporosity. Sample TiGa120 has a lower photocatalytic activity probably due to the high concentration of a photocatalytically inactive Ga phase. The best photocatalytic activity in the UV region ($k = 0.08447$ and $0.08425\,\text{min}^{-1}$) was achieved with the samples TiGa010 and TiGa020, which contain 2.18 and 4.28 wt.% of Ga; a good photocatalytic activity is driven by their mesoporous character [30]. The samples TiGa010 and TiGa020 showed 100% photobleaching of Orange II after 29 and 34 min, respectively. The Ga^{3+}-doped TiO_2 samples had comparable rate constants under the UV irradiation as Ge^{4+} [47] doped TiO_2 and twice higher than In^{3+} [4] doped titania.

The lower photocatalytic activity of titania under Vis light irradiation can be attributed to the increased content of an amorphous phase, worse anatase crystallinity, and an increased band-gap energy. As stated above, the higher concentration of gallium likely increased the amount of a nondiffractive phase (perhaps Ga enriched), which cannot be

Table 2: Rate constant and degree of degradation Orange II dye (90 min.).

Sample	Band-gap (eV)	k 365 nm (min^{-1})	Degree of bleaching (%)	k 400 nm (min^{-1})	Degree of bleaching (%)	200°C k 365 nm (min^{-1})	200°C k 400 nm (min^{-1})
TiGa001	3.10	0.02989	98.5	0.00536	43.9	0.02478	0.00463
TiGa005	3.12	0.01965	82.3	0.00567	45.9	0.03422	0.0047
TiGa010	3.15	0.08447	100*	0.01451	83.1	0.05564	0.00632
TiGa020	3.22	0.08425	100*	0.00833	79.1	0.05226	0.00591
TiGa050	3.21	0.03011	99.1	0.00456	38.9	0.02417	0.00345
TiGa080	3.20	0.01153	67.2	0.00267	23.6	0.01619	0.00398
TiGa100	3.20	0.00769	52.7	0.00186	16.2	0.01406	0.00376
TiGa120	3.20	0.00438	34.6	0.00349	29.2	0.01570	0.00361

Time reaction *29 min, **34 min.

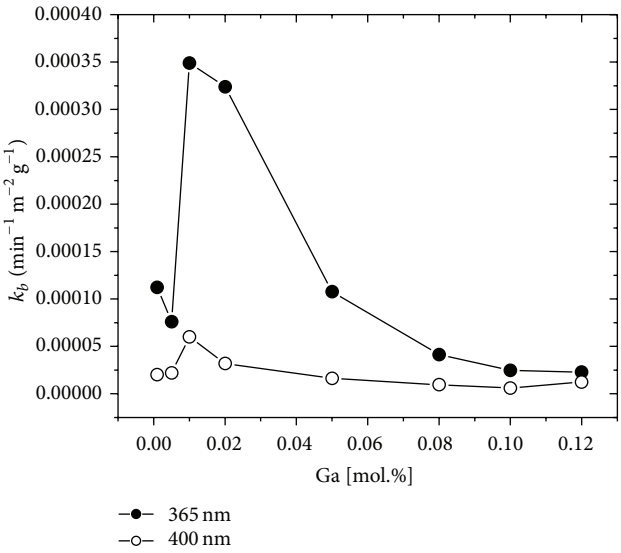

FIGURE 6: Dependence of k_b(k_b = k/BET) on the content of Ga [mol.%].

identified by X-ray diffraction nor Raman spectroscopy, but which was quantified by Rietveld refinement after addition of internal standard. The best photocatalytic activity in the visible-light region has been achieved with the sample labeled TiGa010 (k = 0.01451 min^{-1}), which showed a slight red shift of absorption edge. That specimen had still very small percentage of the nondiffractive component as compared to lower-doped and undoped titania.

Ga^{3+}-doped TiO_2 prepared by homogeneous hydrolysis showed up to 8 times higher photocatalytic activity than the sol-gel-prepared TiO_2 with the Orange II photobleaching rate constant 0.013 min^{-1} [9]. Figure 6 presents dependence of recalculated k_b (k_b = k/BET) on the content of Ga. It is clear that the best photocatalytic activity is determined by the optimum ratio of Ga : Ti in the crystal lattice similarly as in In^{3+}-doped TiO_2 [4]. Annealing at 200°C caused particle growth, which consequently led to bigger areas of photocatalytically inactive domains and secondly to dehydroxylation of the particle surface. Both these facts could consequently reduce the photocatalytic activity (see Table 2).

4. Conclusions

New Ga^{3+}-doped TiO_2 photocatalytic materials were prepared by a homogeneous hydrolysis of titanium oxo-sulphate and gallium(III) nitrate with urea in an aqueous solution. Incorporation of Ga^{3+} into the anatase lattice has a clear positive effect on the photocatalytic activity under UV and Vis light irradiation up to a certain extent of Ga. Ga^{3+} doping had also impact on the size of the crystallites (decrease), surface area (increase), and texture of the samples. Higher amount of gallium led to the formation of a nondiffractive phase with higher content of Ga, which could be photocatalytically inactive. The best degree of conversion (100% after 29 min) for photocatalytic discoloration of Orange II dye had a sample denoted as TiGa010, which contained 2.18 wt.% of Ga. The cost-effective method of homogeneous hydrolysis can be used for preparation of Ga^{3+} titania with potential use for light-assisted oxidation of toxic organic molecules in the surface waters.

Conflict of Interests

The authors declare that there is no conflict of interests regarding the publication of this paper.

Acknowledgments

This work was supported by the RVO 61388980. The authors wish to thank to K. Šafářová of the Regional Centre of Advanced Technologies and Materials, Faculty of Science, Palacký University in Olomouc for providing the HRTEM measurements.

References

[1] K. Y. Jung, S. B. Park, and H. D. Jang, "Phase control and photocatalytic properties of nano-sized titania particles by gas-phase pyrolysis of $TiCl_4$," *Catalysis Communications*, vol. 5, no. 9, pp. 491–497, 2004.

[2] I. Hong, "VOCs degradation performance of TiO_2 aerogel photocatalyst prepared in SCF drying," *Journal of Industrial and Engineering Chemistry*, vol. 12, no. 6, pp. 918–925, 2006.

[3] V. Štengl, V. Houšková, N. Murafa, and S. Bakardjieva, "Synthesis of mesoporous titania by homogeneous hydrolysis of titania oxo-sulfate in the presence of cationic and anionic surfactants," *Ceramics*, vol. 54, no. 4, pp. 368–378, 2010.

[4] V. Štengl, F. Opluštil, and T. Němec, "In3+-doped TiO_2 and TiO_2/In_2S_3 Nanocomposite for photocatalytic and stoichiometric degradations," *Photochemistry and Photobiology*, vol. 88, no. 2, pp. 265–276, 2012.

[5] A. Mattsson, C. Lejon, S. Bakardjieva, V. Štengl, and L. Österlund, "Characterisation, phase stability and surface chemical properties of photocatalytic active Zr and Y co-doped anatase TiO_2 nanoparticles," *Journal of Solid State Chemistry*, vol. 199, pp. 212–223, 2013.

[6] V. Štengl, V. Houšková, S. Bakardjieva, N. Murafa, and P. Bezdička, "Niobium and tantalum doped titania particles," *Journal of Materials Research*, vol. 25, no. 10, pp. 2015–2024, 2010.

[7] V. Štengl, J. Velická, M. Maříková, and T. M. Grygar, "New generation photocatalysts: how tungsten influences the nanostructure and photocatalytic activity of TiO_2in the UV and visible regions," *ACS Applied Materials and Interfaces*, vol. 3, no. 10, pp. 4014–4023, 2011.

[8] V. Štengl and S. Bakardjieva, "Molybdenum-doped anatase and its extraordinary photocatalytic activity in the degradation of Orange II in the UV and vis regions," *Journal of Physical Chemistry C*, vol. 114, no. 45, pp. 19308–19317, 2010.

[9] A. N. Banerjee, S. W. Joo, and B. K. Min, "Photocatalytic degradation of organic dye by sol-gel-derived gallium-doped anatase titanium oxide nanoparticles for environmental remediation," *Journal of Nanomaterials*, vol. 2012, Article ID 201492, 14 pages, 2012.

[10] X. B. Li, Q. Liu, X. Y. Jiang et al., "Enhanced photocatalytic activity of Ga-N Co-doped anatase TiO_2 for water decomposition to hydrogen," *International Journal of Electrochemical Science*, vol. 7, no. 11, pp. 11519–11527, 2012.

[11] M. Hirano and T. Ito, "Titania solid solution nanoparticles co-doped with niobium and gallium," *Journal of the Ceramic Society of Japan*, vol. 118, no. 1384, pp. 1170–1175, 2010.

[12] S. Song, C. Wang, F. Hong, Z. He, Q. Cai, and J. Chen, "Gallium- and iodine-co-doped titanium dioxide for photocatalytic degradation of 2-chlorophenol in aqueous solution: role of gallium," *Applied Surface Science*, vol. 257, no. 8, pp. 3427–3432, 2011.

[13] P. L. Richardson, M. L. N. Perdigoto, W. Wang, and R. J. G. Lopes, "Heterogeneous photo-enhanced conversion of carbon dioxide to formic acid with copper- and gallium-doped titania nanocomposites," *Applied Catalysis B*, vol. 132-133, no. 0, pp. 408–415, 2013.

[14] JCPDS, *PDF 2 Database, Release 50*, International Centre for Diffraction Data, Newtown Square, Pa, USA, 2000.

[15] ICSD, *ICSD Database FIZ Karlsruhe*, 2008.

[16] J. Środoń, V. A. Drits, D. K. McCarty, J. C. C. Hsieh, and D. D. Eberl, "Quantitative X-ray diffraction analysis of clay-bearing rocks from random preparations," *Clays and Clay Minerals*, vol. 49, no. 6, pp. 514–528, 2001.

[17] S. Brunauer, P. H. Emmett, and E. Teller, "Adsorption of gases in multimolecular layers," *Journal of the American Chemical Society*, vol. 60, no. 2, pp. 309–319, 1938.

[18] E. P. Barrett, L. G. Joyner, and P. P. Halenda, "The determination of pore volume and area distributions in porous substances. I. Computations from nitrogen isotherms," *Journal of the American Chemical Society*, vol. 73, no. 1, pp. 373–380, 1951.

[19] A. A. Christy, O. M. Kvalheim, and R. A. Velapoldi, "Quantitative analysis in diffuse reflectance spectrometry: a modified Kubelka-Munk equation," *Vibrational Spectroscopy*, vol. 9, no. 1, pp. 19–27, 1995.

[20] Z. C. Orel, M. K. Gunde, and B. Orel, "Application of the Kubelka-Munk theory for the determination of the optical properties of solar absorbing paints," *Progress in Organic Coatings*, vol. 30, no. 1-2, pp. 59–66, 1997.

[21] V. Štengl, V. Houšková, S. Bakardjieva, N. Murafa, and V. Havlín, "Optically transparent titanium dioxide particles incorporated in poly(hydroxyethyl methacrylate) thin layers," *Journal of Physical Chemistry C*, vol. 112, no. 50, pp. 19979–19985, 2008.

[22] V. Štengl, V. Houškova, S. Bakardjieva, and N. Murafa, "Photocatalytic activity of boron-modified titania under UV and visible-light illumination," *ACS Applied Materials and Interfaces*, vol. 2, no. 2, pp. 575–580, 2010.

[23] H. Lachheb, E. Puzenat, A. Houas et al., "Photocatalytic degradation of various types of dyes (Alizarin S, Crocein Orange G, Methyl Red, Congo Red, Methylene Blue) in water by UV-irradiated titania," *Applied Catalysis B*, vol. 39, no. 1, pp. 75–90, 2002.

[24] A. A. Sattar, "Composition dependence of some physical, magnetic and electrical properties of Ga substituted Mn-ferrites," *Journal of Materials Science*, vol. 39, no. 2, pp. 451–455, 2004.

[25] R. C. Pullar, S. J. Penn, X. Wang, I. M. Reaney, and N. M. Alford, "Dielectric loss caused by oxygen vacancies in titania ceramics," *Journal of the European Ceramic Society*, vol. 29, no. 3, pp. 419–424, 2009.

[26] V. Štengl and T. M. Grygar, "The simplest way to iodine-doped anatase for photocatalysts activated by visible light," *International Journal of Photoenergy*, vol. 2011, Article ID 685935, 13 pages, 2011.

[27] C. Weidenthaler, "Pitfalls in the characterization of nanoporous and nanosized materials," *Nanoscale*, vol. 3, no. 3, pp. 792–810, 2011.

[28] S. Lowell and J. E. Shields, *Powder Surface Area and Porosity*, Chapman and Hall, London, UK, 1998.

[29] J. A. deBoer, *The Shape of Capillaries in the Structure and Properties of Porous Materials*, P. Eisenklam, London, UK, 1958.

[30] V. Štengl, V. Houšková, S. Bakardjieva, and N. Murafa, "Photocatalytic degradation of acetone and butane on mesoporous titania layers," *New Journal of Chemistry*, vol. 34, no. 9, pp. 1999–2005, 2010.

[31] G.-S. Shao, X.-J. Zhang, and Z.-Y. Yuan, "Preparation and photocatalytic activity of hierarchically mesoporous-macroporous $TiO_{2-x}N_x$," *Applied Catalysis B*, vol. 82, no. 3-4, pp. 208–218, 2008.

[32] P. A. Connor, K. D. Dobson, and A. James McQuillan, "Infrared spectroscopy of the TiO_2/aqueous solution interface," *Langmuir*, vol. 15, no. 7, pp. 2402–2408, 1999.

[33] G. V. Jere and C. C. Patel, "Infrared absorption studies on peroxy titanium sulphate," *Canadian Journal of Chemistry*, vol. 40, no. 8, pp. 1576–1578, 1962.

[34] R. Nakamura, A. Imanishi, K. Murakoshi, and Y. Nakato, "In situ FTIR studies of pimary intermediates of photocatalytic reactions on nanocrystalline TiO_2 films in contact with aqueous solutions," *Journal of the American Chemical Society*, vol. 125, no. 24, pp. 7443–7450, 2003.

[35] M. Ignat, L. M. Revenco, A. R. Pascaru, and E. Popovici, "Functionalized zeolitic materials with photocatalytic properties," *Acta Chemica*, vol. 19, pp. 21–34, 2011.

[36] M. Pal, U. Pal, J. M. G. Y. Jiménez, and F. Pérez-Rodríguez, "Effects of crystallization and dopant concentration on the emission behavior of TiO_2: Eu nanophosphors," *Nanoscale Research Letters*, vol. 7, article 1, pp. 1–12, 2012.

[37] G. Liu, C. Sun, H. G. Yang et al., "Nanosized anatase TiO_2 single crystals for enhanced photocatalytic activity," *Chemical Communications*, vol. 46, no. 5, pp. 755–757, 2010.

[38] J.-H. Yi, C. Bernard, F. Variola et al., "Characterization of a bioactive nanotextured surface created by controlled chemical oxidation of titanium," *Surface Science*, vol. 600, no. 19, pp. 4613–4621, 2006.

[39] J. Chae, J. Lee, J. H. Jeong, and M. Kang, "Hydrogen production from photo splitting of water using the Ga-incorporated TiO(2)s prepared by a solvothermal method and their characteristics," *Bulletin of the Korean Chemical Society*, vol. 30, no. 2, pp. 302–308, 2009.

[40] K. M. Reddy, S. V. Manorama, and A. R. Reddy, "Bandgap studies on anatase titanium dioxide nanoparticles," *Materials Chemistry and Physics*, vol. 78, no. 1, pp. 239–245, 2003.

[41] H. Yuan and J. Xu, "Preparation, characterization and photocatalytic activity of nanometer SnO_2 ," *International Journal of Chemical Engineering and Applications*, vol. 1, no. 3, pp. 241–246, 2010.

[42] P. Mäkie, P. Persson, and L. Österlund, "Solar light degradation of trimethyl phosphate and triethyl phosphate on dry and water-precovered hematite and goethite nanoparticles," *The Journal of Physical Chemistry C*, vol. 116, no. 28, pp. 14917–14929, 2012.

[43] E. Sanchez and T. Lopez, "Effect of the preparation method on the band gap of titania and platinum-titania sol-gel materials," *Materials Letters*, vol. 25, no. 5-6, pp. 271–275, 1995.

[44] N. Serpone, D. Lawless, and R. Khairutdinov, "Size effects on the photophysical properties of colloidal anatase TiO_2 particles: size quantization or direct transitions in this indirect semiconductor?" *Journal of Physical Chemistry*, vol. 99, no. 45, pp. 16646–16654, 1995.

[45] D. S. Bhatkhande, V. G. Pangarkar, and A. A. Beenackers, "Photocatalytic degradation for environmental applications: a review," *Journal of Chemical Technology and Biotechnology*, vol. 77, no. 1, pp. 102–116, 2002.

[46] S.-A. Lee, J.-Y. Hwang, J.-P. Kim, C.-R. Cho, W.-J. Lee, and S.-Y. Jeong, "Metal/insulator/semiconductor structure using Ga_2O_3 layer by plasma enhanced atomic layer deposition," *Journal of the Korean Physical Society*, vol. 47, no. 2, pp. S292–S295, 2005.

[47] V. Stengl, T. M. Grygar, J. Velická, J. Henych, and S. Bakardjieva, "Impact of Ge^{4+} ion as structural dopant of Ti^{4+} in anatase: crystallographic translation, photocatalytic behavior, and efficiency under UV and VIS irradiation," *Journal of Nanomaterials*, vol. 2012, Article ID 252894, 11 pages, 2012.

[48] V. Stengl, T. M. Grygar, J. Henych, and M. Kormunda, "Hydrogen peroxide route to Sn-doped titania photocatalysts," *Chemistry Central Journal*, vol. 6, article 113, 2012.

[49] M. Toyoda, Y. Nanbu, Y. Nakazawa, M. Hirano, and M. Inagaki, "Effect of crystallinity of anatase on photoactivity for methyleneblue decomposition in water," *Applied Catalysis B*, vol. 49, no. 4, pp. 227–232, 2004.